https://doi.org/10.3311/PPci.19642

Periodica Polytechnica Civil Engineering, 66(3), pp. 681–693, 2022

Damage Propagation at the Interface of a Sandwich Beam

Imane Hammoudi[1*], Mokhtar Touati[1], Mohamed Chabaat[1]

[1] Built Environmental. Research Lab., Department of Structures and Materials, Civil Engineering Faculty, University of Sciences and Technology Houari Boumediene (U.S.T.H.B.), B. P. 32 El-Alia, Bab Ezzouar, 16111 Algiers, Algeria
[*] Corresponding author, e-mail: ihammoudi@usthb.dz

Received: 05 December 2021, Accepted: 12 March 2022, Published online: 29 March 2022

Abstract

In this research work, damage propagation at the interface of a cracked sandwich beam is considered. The behavior of Sandwich Beams (SB) depends upon a law based on relationship between tangential or normal efforts with inelastic propagation. As the crack propagates; fracture parameters such as stress intensity factors and energy release rates corresponding to the applied shear stress in mode I and II are determined. Linear and nonlinear models are presented. It is shown that the Timoshenko beam's theory is employed in the formulation of transverse shear and peel stresses at the overlap ends. These parameters are used to derive energy release rates. Besides, effects of the adhesive thickness and shear modulus on the shear and peel stresses in the adhesive are studied. Obtained results from the analytical solution for the case of a sandwich beam at the interface (adhesive part) agree well with numerical investigations available in the literature. It is also proven that the contribution of the adhesive bond to the energy release rate increases for softer adhesives, shorter cracks and thicker bonds.

Keywords

sandwich beam, shear stress, stress intensity factor, energy release rate

1 Introduction

Nowadays, many industrial sectors (automotive, aeronautical, naval and others) are researching and experimenting new materials. These materials must provide structures that are increasingly light and strong to achieve the broader goal of attaining greater speeds with less energy consumption. However, in actual products, there are other components and parts that are made of steel or Aluminum, wood alloys that must be joined to the composite material using in the building and civil engineering (housing cells, factory chimneys, formwork, shelter, swimming pool, wall panel, profiles…).

Recently the replacement of the traditional materials by the sandwiches is motivated by the lightening of the structures having the same mechanical properties or higher. An important effort was deployed this last decade to extend the life of the structures in sandwich materials and also to prevent them from failure. Composite materials considered in this study are classified as mixed beams or three-layer sandwich materials. These structural systems are governed by the same nature of differential equations, both in the plane and the off-plane behavior. Partially connected multi-layers are typically encountered in the field of wood construction, where the elements are assembled by bolting or gluing. In the construction field, composite steel or concrete wood beams are commonly used, for their optimum overall mechanical and economic properties. The formalism of the theory of the behavior in the plan and out of plane of mixed beams is given and obtained results and their interpretation are proposed for mixed beams of a rectangular section and simply supported. These results are analogous to those obtained for vibrations in the plane for both composite beams and sandwich girders where frequencies increase with the rigidity of the connection. The treatment of more complex loading conditions is analyzed from numerical procedures, such as finite element method.

Stresses in cement lap joints (adhesive) were first determined by Goland and Reissner [1]. They elaborated a new method on composite materials such as wood and metal sheets using the cement lap adhesives as a very strong bond. Also, they were able to assess loads and stresses at the edges of the joints for cylindrically bent plates using the method of finite deflection theory. Besides, Goland and Reissner took into consideration the effect of the deflection at the jointed members due to the plate bending and also the effect of the tearing stress that was neglected before.

Cite this article as: Hammoudi, I., Touati, M., Chabaat, M. "Damage Propagation at the Interface of a Sandwich Beam", Periodica Polytechnica Civil Engineering, 66(3), pp. 681–693, 2022. https://doi.org/10.3311/PPci.19642

Using a similar procedure to Goland and Reissner, Luo and Tang [2] presented a new formulation with an analytical solution for adhesive bonded composite lap joints, taking into consideration the transverse shear deformation as well as the large deflection in adherents. They obtained the peel stress of adhesive and were able to predict the peel stress in the bending line. This work is based on a simple model of the mechanics of a composite.

In order to compare their results obtained geometrically using a nonlinear finite element method to those from an analytical solution, Tsai and Morton [3] introduced a generalized state-based theory that overcomes the limitations of the original theory and stated that the difference between short and long joints can be defined on the basis of the impact of the large overlap deflection on the edge moment. It is shown that for the short joint, K–ξ curves are intensive to the adhesive thickness not to the material property; however, these curves are important to both factors for the long joint. The modification of theoretical solutions has been corrected for practical applications. For a review concerning the argument of validity and its major applications, the reader is referred to the work of Tsai and Morton [3].

The beam theory for modeling adhered bending response and made real model than Goland and Reissner by adding the effects of bend shear strains was due to Oplinger [4]. This work supposed incomplete because the effect of bond thickness deformation was ignored by Goland and Reissner. It was also proven that Oplinger's models gave a more reasonable approximation for the long single lap joint for different thicknesses and material properties in the adhesive layer.

In a recent research work, both numerical simulations and experimental tests have been performed on single lap-shear joints made of carbon–epoxy laminated composites and an epoxy adhesive [5]. This work was able to verify the adequacy of cohesive damage models for the strength prediction of bonded joints. Authors proposed a mixed-mode cohesive damage model to simulate damage onset and growth in the adhesive layer. Tensile tests were performed for joints with different overlap lengths and obtained numerical simulations described with a reasonable accuracy the mechanical behavior of the joints tested.

A Cohesive Zone Model (CZM) was adapted to model the propagation of cracks in bonded joints, using a bilinear traction-separation law implemented in the finite element code ABAQUS. The riveted assemblies were modeled with the XFEM damage method identified in this ABAQUS numerical code. Both CZM and XFEM methods are combined to model hybrid assemblies. The results were consistent with the experimental results and made it possible to guarantee the validity of the applied numerical model [6]. On the other hand, generated robust and physically reasonable Abaqus-based FEA solutions to model multi-step damage processes in laminated composite materials and structures were presented by Kim et al. [7]. They demonstrated their efficiency on representative examples.

Recently, a free vibration of a cracked cantilever bar was investigated using an Approximate Analytical approach [8, 9]. The crack is modeled by an equivalent axial spring with stiffness Kx according to Castigliano's theorem. The effect of different crack depth ratio on the longitudinal frequencies and mode shapes in the cracked bar has been analyzed. Authors have shown that an increase in the crack depth ratio produces a decrease in the fundamental longitudinal natural frequency of a cracked bar. On the other hand, approximate analytical results indicate that the variation of a normalized longitudinal natural frequency with respect to the crack depth ratio give comparable results with those obtained from the numerical solution of an analytical equation of a cracked beam.

Failure occurs due to the formation of localized macrocracks that occurs through the coalescence of diffuse microcracks surround the tip of the main crack [10]. In this research work, authors evaluated the energy release rates during the propagation of a crack in the presence of a dislocation in the vicinity of the crack's tip. The problem was formulated using a composite material and they have shown throughout their study that by using a numerical approaches such as FEM along with the software ABAQUS, the stress field and stress intensity factor are determined for different crack lengths. Besides, energy release rate during crack propagation are calculated. In a recent research work, Ayas et al. [11] estimated the von Mises stress distribution around the crack tip under mixed modes I and II during the propagation of a crack interacting with two nearby circular inclusions. Using numerical techniques, they were able to assess SIFs for different crack lengths in a brittle material.

The size and shape of the damage zone has been determined numerically by Hamli Benzahar and Chabaat [12]. They have studied the damage zone length limit during the crack propagation in brittle materials. Their work was mainly based on the determination of stress fields by varying the distance between a semi-infinite crack and a neighboring dislocation. They have proven that for a given position between the two cracks (semi-infinite crack and dislocation), stress fields are obtained that lead to a limiting damage zone length.

A crack propagation in composite beams where the bending of an elastic-composite beam with interlayer slip, has been theoretically investigated by Hammoudi and Chabaat [13]. They derived governing equations for layered beams (mechanically jointed) considering shear connections (lap joints mechanically or adhesively jointed) and sandwich constructions (with weak shear cores). In their study, composite beams were subjected to end moments with interlayer slip in the interface. They have proven that a boundary layer prevails at the beam extremity for a very stiff connection.

On the other side, a finite element plate model with displacement formulation is presented for the analysis of thin and thick plates in the nonlinear domain by Lyamine [14]. The latter is an isotropic rheological model based on Reissner theory [1] with the consideration of transverse shear. The material nonlinearity considered is of the elastoplastic type and the resulting systems of equations are solved using an iterative incremental approach. This work made it possible to demonstrate the good performance of the heterosis element compared to standard plate elements.

Based on the analysis of crack growth of End-Notch Flexure (ENF) specimens, it is found that interlaminar shear deformation may influence the evaluation of the Mode II fracture toughness [15]. The influence may, however, be minimized by using beams with a small thickness-to-crack length ratio. On the other hand, the design analysis presented for sizing the ENF specimen dictates that a minimum thickness has to be used in order to maintain linear behavior. For geometries and material properties commonly in use (unidirectional lay-ups), the error in the toughness value, calculated from measured experimental values, induced by neglecting interlaminar shear deformation is less than ten percent according to this analysis. Besides, the interlaminar fracture toughness in mode II and mode III of a number of advanced composites was studied using beam type test specimens and scanning electron microscopy [16]. Special emphasis was placed on elucidating the material aspects of the fracture process and on quantifying the effect of matrix on fracture energy.

The fracture energy in mode II was independent of crack extension while mode III exhibited a rather probabilistic "resistance" behavior that was attributed to the effect of fiber bridging.

The use of Carbon Fiber-Reinforced Polymer (CFRP) composites in strengthening reinforced Concrete Beams (CB) have been widely utilized for external flexural or shear reinforcement in construction. Ibrahim and Rad [17] developed a numerical model from testing several beams in bending to determine the concrete contribution to their shear resistance. A series of numerical simulations have been carried out on non-prismatic RC beams having different haunch angle. Comparing between numerical and experimental results, authors showed that changing beams geometry can have an impact on the shear strength. It was also proven that CFRP strips applied to the critical sections surface will enhance the shear strength of RC beams.

In this research study, Timoshenko beam theory for equilibrium equations of adherents with analytical solutions for force boundary conditions at both overlap ends is considered. These equations are derived on the basis of a geometrically nonlinear analysis for infinitesimal elements of adherend and adhesive material. Besides, equations formulation based on the Timoshenko beam's theory [18] can be applied to isotropic and composite single lap joint. However, it is considered better than Euler beam's theory based on the formulation for only composite single lap joints, particularly edge moment factor and peel stress. The present formula of peel stress gave excellent numerical results for mixed-modes I and II. Besides, energy release rates (ERR) have been validated for selected results available in the literature. Shear stress and stress intensity factor (SIF) of the adhesive are also determined from Timoshenko beam's theory. Throughout this study, we proceed as follows: The problem is divided in two parts: First, shear stresses at the edge and along the adhesive part are computed and second, energy release rates of the composite beam are developed.

2 Model description

Consider the sandwich beam (SB) shown in Fig. 1. Under normal applied load F (mode I) and shear force P (mode II), a crack in the adhesive bond advances along the plane of symmetry. Since the adhesive bond is usually softer and thinner than the adherend, the system of each arm of the adherend and the adhesive bond can be modelled as a Cantilever Beam (CB). The initial crack renders the beam partially free in one edge and fixed or rolled in the other edge. In this study, the following characteristics are considered:

l: Crack length; B: Specimen width; h: Adherend height;

$2t$: Adhesive thickness; E_1, v_1: Young's modulus and Poisson's coefficient of the adherend, respectively.

E_2, v_2: Young's modulus and Poisson's coefficient of the adhesive, respectively. F: Tearing force; P: Shearing force.

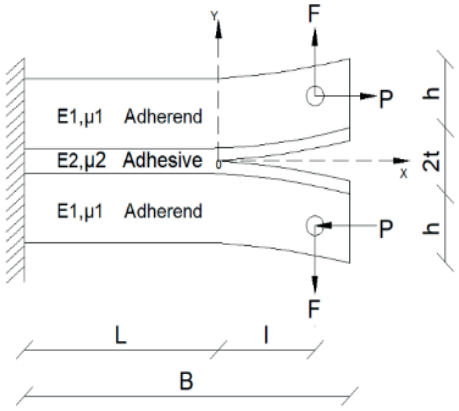

Fig. 1 Proposed model

3 Hypothesis

For the present study, some hypotheses should be taken in consideration:

- Adherent and adhesive are considered as nonlinearly elastic.
- $E_1 > E_2$;
- Mixed mode (I + II).
- Plane stress.
- Isotropic adherent.
- The displacement of the composite beam determinate by the flexion of the beam.

4 Basic equations

Basic equations for the overlap and outer adherend are written according to the Fig. 1. This latest gives the basic parameters of a beam in its lower and upper part which corresponds to the adherend. On the other side, the adhesive considered in the middle has an edge crack.

4.1 Loads at the edge of the beam

The edge part of the beam is submitted to two forces: a shearing force P and a tearing force F as shown in Fig. 2. Since the beam is symmetrical, the equilibrium equations of the beam are given as follows;

$$R_A + F = 0\,, \tag{1}$$

$$N_A - P = 0\,, \tag{2}$$

$$M_A + F.B - P.\left(t + \frac{h}{2}\right) = 0\,. \tag{3}$$

4.2 Deflection beam

The deflection is schematically represented in Fig. 3. The bending moment in section 1-1 at the edge is w_0;

$$M_0^g(x) = R_A(x) - N_A(w_0) + M_A,\ -L < x < 0\,, \tag{4}$$

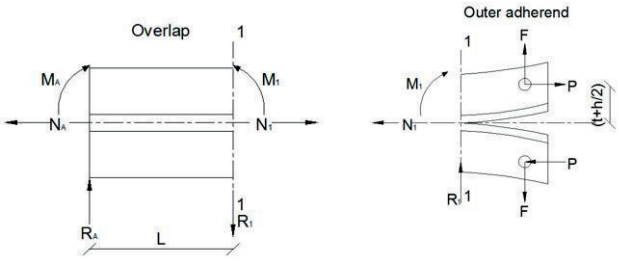

Fig. 2 Decomposition of the beam under loading, reaction forces in section 1-1

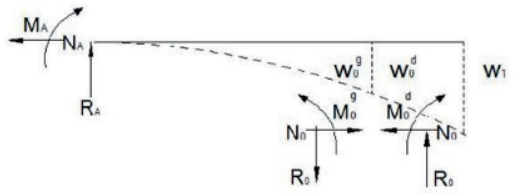

Fig. 3 Deflection in the beam

$$M_0^d(x) = -M_A - R_A(L + x) + N_A(w_1),\ O < x < -l\,, \tag{5}$$

$$M_1(x) = M_A + R_A(x) - N_A(w_2),\ 0 < x < B\,. \tag{6}$$

The relation of bending moment based on Timoshenko's beam theory is as follows;

$$M_0^g = -D_0.\frac{d^2 w_0}{dx_0^{\,2}}\,, \tag{7}$$

$$M_0^d = -D_1.\frac{d^2 w_1}{dx_1^{\,2}}\,, \tag{8}$$

$$M_1 = -D_2.\frac{d^2 w_2}{dx_2^{\,2}}\,, \tag{9}$$

where, D_0, D_1 and D_2 are the bending stiffness of the outer adherend and overlap.

Substituting Eq. (7) through Eq. (9) into simultaneous Eq. (4) to Eq. (6), we get;

$$w_0^g = A_1 \sinh \beta_0 x_0 + A_2 cosh \beta_0 x_0 + \frac{M_A}{F} + \frac{R_A}{F} x_0, \tag{10}$$

$$w_0^d = B_1 \sinh \beta_1 x_1 + B_2 cosh \beta_1 x_1 - \frac{M_A}{F}\,, \tag{11}$$

$$w_1 = C_1 \sinh \beta_2 x_2 + C_2 cosh \beta_2 x_2 + \frac{M_A}{F} + \frac{R_A}{F} x_2\,. \tag{12}$$

Here; A_1, A_2, B_1, B_2, C_1, C_2, are unknown integration constants to be determined using boundary conditions, and constants β_0, β_1, β_2 are computed by the following equations;

$$\beta_0 = \sqrt{\frac{F}{D_0}},\ \beta_1 = \sqrt{\frac{F}{D_1}},\ \beta_2 = \sqrt{\frac{F}{D_2}}\,. \tag{13}$$

It is noted that in Eq. (10) to Eq. (12), there are six integration constants and two reactions to be determined. Then, one needs to have 8 independent equations, two equilibrium equations such as those given in Eq. (1) and Eq. (2), and two more equations from the deformation continuity in section 1-1 as follow;

$$U_0^d(l) = U_0^g(-L),\ w_0^d(l) = w_0^g(-L), \tag{14}$$

$$\frac{dw_0^d(l)}{dx_0} = \frac{dw_0^g(-L)}{dx_0}, \tag{15}$$

$$2U_S = U_2 + U_1,\ 2w_S = w_2 - w_1,\ 2U_S = U_2 - U_1. \tag{16}$$

5 Overlap and adhesive stresses

The upper and lower adherends are identical and symmetrical. To obtain the solution of shear and peel stress, the following boundary conditions (BC) are considered:

$$\begin{aligned} &2N_S = N_2 + N_1,\ 2Q_S = Q_2 - Q_1,\ 2M_S \\ &\quad = M_2 - M_1,\ 2wa = w2 + w1, \end{aligned} \tag{17}$$

$$2N_a = N_2 - N_1,\ 2Q_a = Q_2 + Q_1,\ 2M_a = M_2 + M_1. \tag{18}$$

5.1 Linear analysis of adhesive joints

Equilibrium equations of adherends 1 in the overlap can be obtained from Fig. 4 as follows;

$$\frac{dN_1}{dx} + \tau = 0,\ \frac{dQ_1}{dx} + \sigma = 0,\ \frac{dM_1}{dx} + \tau.\frac{h}{2} - Q_1 = 0, \tag{19}$$

$$\frac{dN_2}{dx} - \tau = 0,\ \frac{dQ_2}{dx} - \sigma = 0,\ \frac{dM_2}{dx} + \tau.\frac{h}{2} - Q_2 = 0, \tag{20}$$

where σ and τ are the peel and shear stress, respectively.

Substitution of Eq. (16) through Eq. (18) into Eq. (19) and Eq. (20) leads us to the following expressions similar to those given in [1];

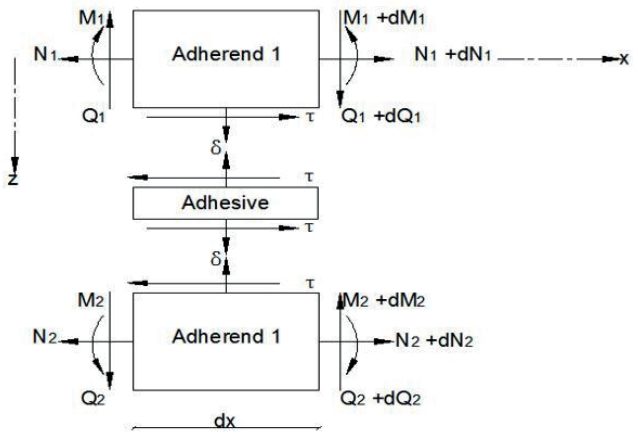

Fig. 4 Stress linear analysis of adhesive joints

$$\tau = \frac{G_a}{2t}\left((U_2 - U_1) + \frac{h}{2}\left(\frac{dw_1}{dx} + \frac{dw_2}{dx}\right)\right), \tag{21}$$

$$\sigma = \frac{E_a(w_2 - w_1)}{2t}, \tag{22}$$

where E_a and G_a are Young's modulus and shear's modulus of the adhesive, respectively.

Using separately Eqs. (19) and (20), Equilibrium equations can take the following form;

$$\frac{dN_s}{dx} = 0,\ \frac{dQ_s}{dx} = 0,\ \frac{dM_s}{dx} = 0, \tag{23}$$

$$\frac{dN_a}{dx} - \tau = 0,\ \frac{dQ_a}{dx} = 0,\ \frac{dM_a}{dx} + \tau\frac{h}{2} - Q_a = 0, \tag{24}$$

$$\tau = \frac{G_a}{t}\left[(U_a) + \frac{h}{2}\left(\frac{dw_a}{dx}\right)\right]. \tag{25}$$

Constitutive relations of Euler beam are given as;

$$N = A_1\frac{du}{dx},\ M = -D_0\frac{d^2w}{dx^2}, \tag{26}$$

where A_1 is an extensional stiffness of the adherends.

If we substitute Eq. (26) into Eq. (25) then, differential equations for shear and peel stress can be written as follows;

$$\frac{d^3\tau}{d^3x} = \frac{G_a}{A_1 t}\left(1 + \frac{h^2}{4}\frac{A_1}{D_0}\right)\frac{d\tau}{dx}, \tag{27}$$

$$\frac{d^4\sigma}{d^4x} + \frac{2E_a}{D_0 t}\sigma = 0. \tag{28}$$

Solutions for the above equations are given as;

$$\tau = A_1\sinh\beta_a x + A_2\cosh\beta_a x + A_3, \tag{29}$$

$$\begin{aligned} \sigma = {} & B_1\sinh\beta_\sigma\sin\beta_\sigma x + B_2\sinh\beta_\sigma\sin\beta_\sigma x + \\ & B_3\cosh\beta_\sigma x\cos\beta_\sigma x + B_4\cosh\beta_\sigma x\cos\beta_\sigma x, \end{aligned} \tag{30}$$

in which integration constants can be determined by the boundary conditions of the overlap (Appendix A) as follows;

$$\alpha_a = \frac{(1+\alpha_k)}{4},\ \alpha_k = \frac{A_1h^2}{4D_0}, \tag{31}$$

$$\beta_a^2 = \alpha_a\beta_\tau^2,\ \beta_\tau = \sqrt{\frac{G_a}{A_1 t}},\ \beta_\sigma = \frac{\sqrt{2}}{2}\sqrt[4]{\frac{E_a}{D_0 t}}, \tag{32}$$

- For isotropic adherents $\alpha_a = 1$ and $\alpha_k = 3$.

Let us substitute Eq. (25) and Eq. (26) into Eq. (23), then, differential equations for adherend displacements take the following form;

$$-\frac{d^4 w_a}{dx^4}+\frac{h}{2}\frac{G_a}{D_0 t}\left(\frac{du_a}{dx}+\frac{h}{2}\frac{d^2 w}{dw^2}\right)=0\,, \tag{33}$$

$$\frac{d^2 u_a}{dx^4}-\frac{G_a}{A_1 t}\left(u_a+\frac{h}{2}\frac{dw_a}{dw^2}\right)=0\,, \tag{34}$$

$$\frac{du_s^2}{dx^2}=0,\;\; D_0\frac{dw_s^4}{dx^4}-\frac{E_a w_s}{t}=0\,. \tag{35}$$

5.2 Nonlinear analysis of adhesive joints

Equilibrium equations of adherend 1 in the overlap can be obtained from Fig. 5;

$$\frac{dN_a}{dx}=0,\;\; \frac{dQ_a}{dx}-\tau\frac{dw_s}{dx}=0,\;\; \frac{dM_a}{dx}+\tau\frac{h}{2}-Q_a = N_s\frac{dw_a}{dx}-N_a\frac{dw_s}{dx} \tag{36}$$

The nonlinear constitutive relations of Euler beam are;

$$\frac{d^2 M_s}{dx^2}=\frac{dQ_s}{dx}-N_s\frac{d^2 w_s}{dx}-N_a\frac{d^2 w_a}{d^2 x}\,, \tag{37}$$

$$\frac{d^2 M_a}{dx^2}=-\frac{h}{2}\frac{d\tau}{dx}+\frac{dQ_a}{dx}-N_s\frac{d^2 w_a}{dx^2}-N_a\frac{d^2 w_s}{d^2 x}\,, \tag{38}$$

with;

$$N_a=A_1\frac{du_a}{dx},\;\; N_s=A_1\frac{du_s}{dx}\,. \tag{39}$$

If we substitute Eq. (39) into Eq. (38), then; equations of adherend's displacements in the overlap become;

$$\frac{d^2 u_s}{dx^2}=0\,, \tag{40}$$

$$-D_0\frac{d^4 w_s}{dx^4}-\frac{E_a}{t}w_s=0\,, \tag{41}$$

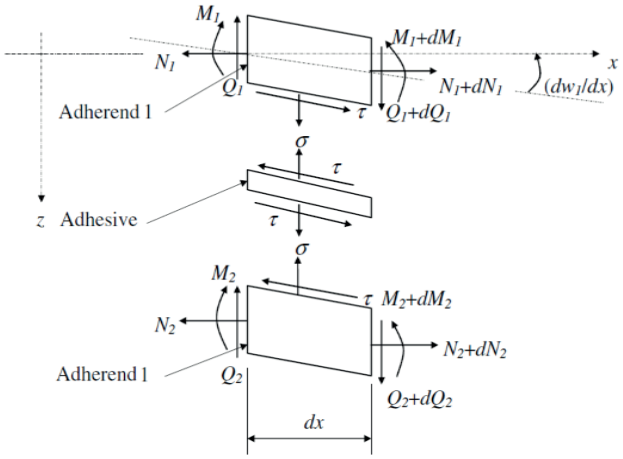

Fig. 5 Stress non-linear analysis of adhesive joints

$$-D_0\frac{d^4 w_a}{dx^4}=-\frac{h}{2}\frac{G_a}{t}\left(\frac{du_a}{dx}+\frac{h}{2}\frac{d^2 w_a}{dx^2}\right)+\frac{E_a}{t}w_a\,, \tag{42}$$

$$A_1\frac{d^2 u_a}{dx^2}-\frac{G_a}{t}\left(du_a+\frac{h}{2}\frac{dw_a}{dx}\right)=0\,. \tag{43}$$

Analytical solutions for Eq. (40) to Eq. (43) are given under the following form;

$$u_s=A_{s1}x+A_{s2}\,, \tag{44}$$

$$w_s=(B_{s1}x\sinh\beta_{s1}x+B_{s2}x\cosh\beta_{s1}x)+(B_{s3}x\sinh\beta_{s1}x+B_{s4}x\cosh\beta_{s1}x), \tag{45}$$

$$u_a=A_{a1}x+A_{a2}\,, \tag{46}$$

$$w_a=B_{a1}\sinh\beta_{a1}x+B_{a2}\cosh\beta_{a1}x+B_{a3}\sinh\beta_{a2}x+B_{a4}\cosh\beta_{a1}x+B_{a5}x+B_{a6}\,. \tag{47}$$

6 Shear and peel stresses

For prescribed force boundary conditions with free fixed ends, symmetrical shear stresses and peel stresses are found as;

$$\tau=\frac{3\beta_\tau}{h}\left(Fh+12M_1\right)\cosh\beta_\tau x+\frac{3\beta_\tau}{h}\left(Fh+12M_1\right), \tag{48}$$

$$\sigma=\frac{E_a}{2t}\left(B\sigma_1\cosh\beta s_{1x}+B\sigma_2\cosh\beta s_{2x}\right). \tag{49}$$

From the above Eqs, we deduce the following stresses;

$$\sigma_{max}=1+\frac{\beta_k}{\beta_\sigma}\coth\beta_k L\,, \tag{50}$$

$$\tau_{max}=\frac{3\beta_\tau}{h}\left(Fh+12M_1\right)\cosh\beta_{\tau 1}L+\frac{3\beta_\tau}{h}\left(Fh+12M_1\right)\cosh\beta_{\tau 2}L. \tag{51}$$

7 Energy release rates

Once the maximum adhesive stresses are obtained, energy release rate G_I and G_{II} are determined according to the following expressions;

$$G_I=\frac{t}{E_a}\left(\sigma_{max}\right)^2, \tag{52}$$

$$G_{II}=\frac{t}{G_a}\left(\tau_{max}\right)^2, \tag{53}$$

$$G_I=\frac{t}{E_a}\left(1+\frac{\beta_k}{\beta_\sigma}\coth\beta_k L\right)^2, \tag{54}$$

$$G_{II} = \frac{t}{G_a}\left(\begin{array}{l}\frac{3\beta_\tau}{h}\left(Fh+12M_1\right)\cosh\beta_{\tau 1}L \\ +\frac{3\beta_\tau}{h}\left(Fh+12M_1\right)\cosh\beta_{\tau 2}L\end{array}\right)^2. \quad (55)$$

Energy release rates for both modes can be written in a dimensional form as; (56)

$$\frac{G_{II}}{GI} = \frac{E_a}{G_a}\left(\frac{\left(\frac{3\beta_\tau}{h}\left(Fh+12M_1\right)\cosh\beta_{\tau 1}L+\frac{3\beta_\tau}{h}\left(Fh+12M_1\right)\cosh\beta_{\tau 2}L\right)^2}{\left(1+\frac{\beta_k}{\beta_\sigma}\coth\beta_k L\right)^2}\right).$$

8 Numerical results and discussions

For the case of Double Cantilever Beam with fixed-Free BC and symmetrical adherents, the following input data in the following Table 1 are considered.

The value of tensile force is estimated to 659.6 N/mm (after [2]).

Fig. 6 shows both moments at the crack tip of DCB with fixed free conditions and also for roller-roller conditions. One can notice that the moment at the crack's tip is very important in DCB when the rate L/l increases. On the other side; the moment is lower for the case of the roller-roller condition and much smaller for the DCB with fixed free BC.

Fig. 7 represents an evaluation of shear stress at the crack tip of DCB with fixed free condition. One can notice that the shear stress increases linearly with the crack's length. It becomes important at the extremity of DCB while the shear stress for the case of a roller- roller BC gets lower for a longer crack's length. This particular case has been proved in the work of [2] et more precisely for the case of fixed free BC.

The peel stress at the crack tip of DCB for fixed free condition increases linearly at the same rate with an increase of crack's lengths. However; the peel shear stress with roller-roller BC gets a higher value for greater crack's lengths. Besides, the peel stress is not important at fixed free BC compared to the roller-roller BC as shown in Fig. 8.

In Fig. 9, contribution of energy G_I to the adhesive layer of the DCB is considered a crucial parameter in the stress evaluation at the crack tip. Energy has a high concentration

Table 1 Geometrical dimensions and mechanical characteristics [2]

Geometrical Dimensions	Mechanical Characteristics
h = 1.6 mm	E_1 = 70 GPA
l = 1.25*L	E_2 = 0.04*E_1
t = 0.078*h	μ_1 = 0.34
L = 32*h	μ_2 = 0.4
	G_a = 10 GPA

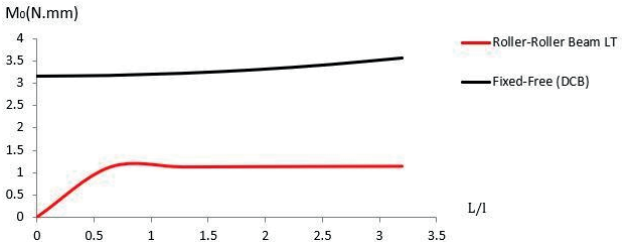

Fig. 6 Moment M_0 at crack tip vs. L/l with fixed-free boundary conditions

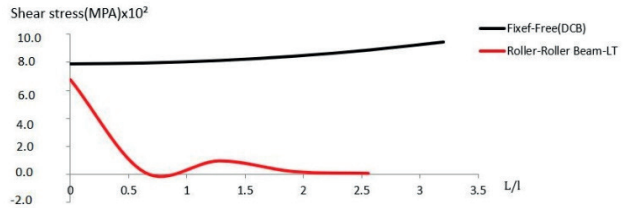

Fig. 7 Shear stress at crack tip vs. L/l with fixed-free conditions

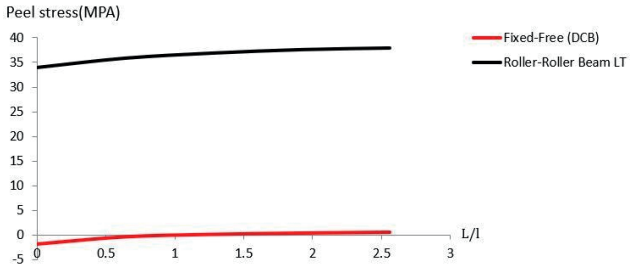

Fig. 8 Peel stress at crack tip vs. L/l with fixed-free conditions

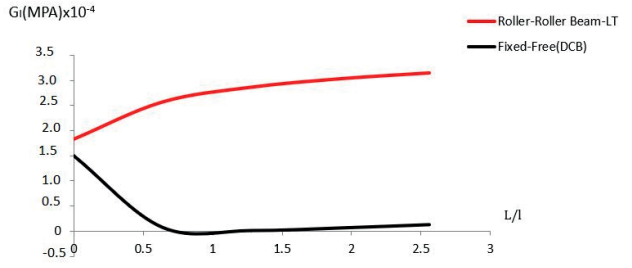

Fig. 9 Energy release rate stress vs. L/l with fixed-free conditions

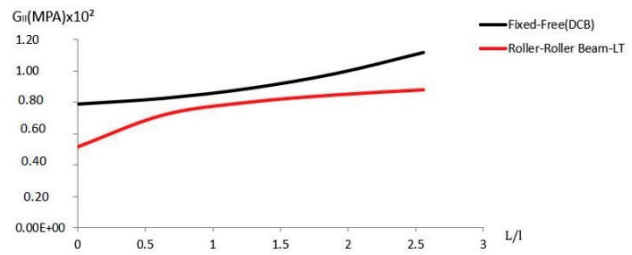

Fig. 10 Energy release rate G_{II} for shear stress vs. L/l with fixed-free conditions

of stress at the tip and decreases for longer crack's lengths. As shown in Fig. 9, the energy contribution to the adhesive layer at the roller-roller BC has a big effect for longer crack's lengths. It is noticed that G_I increases and becomes very important for fixed free condition.

In Fig. 10, contribution of energy G_{II} to the adhesive layer of the DCB increases with increasing cracks lengths at fixed free boundary condition, however the contribution of energy to the adhesive layer at the roller-roller boundary condition increases with a slight increase in the crack's length. In the other hand, it gets lower than the energy for fixed free boundary conditions.

In Fig. 11, contribution of energy release rates G_{II}/G_I for both modes to the adhesive layer of the DCB increases in a proportional way with the cracks length at fixed free BC, however the energy's contribution to the adhesive layer at the roller-roller condition decreases for longer crack's length. It reaches a pick at half crack's length. This energy is lower than the one for the case of fixed free conditions.

Effect of the adhesive modulus on the ERR is illustrated in Fig. 12 which shows the dependency of G_{II}/G_I on the relative stiffness for various crack lengths. The contribution of the adhesive bond is larger for shorter cracks and, of course, for softer adhesives. On the other hand, an increase in the energy is accompanied by an increase in the ratio E_{II}/E_I however; the energy to the adhesive layer at the roller-roller BC increases for longer crack lengths, but it is lower than the energy for the case of fixed free BC.

Plots of G_I as a function of the bond thickness t normalized with respect to the adherend height h is shown in Fig. 13 for fixed free conditions. It is noticed that G_I is independent of the bond thickness and decreases when the ratio of t/h of adhesive increases at the fixed free BC. It is also noticed that the contribution of energy to the adhesive layer at the roller-roller BC increases for longer crack's lengths, but it gets lower than the energy for fixed free boundary conditions.

Fig. 14 represents the energy G_{II} to the adhesive layer of the DCB. It is shown that the energy G_{II} decreases drastically for smaller ratio of t/h of adhesive but increases at fixed free boundary condition. The contribution of energy to the adhesive layer at the roller-roller BC gets steady for longer crack's lengths, but it's lower than the energy of fixed free BC.

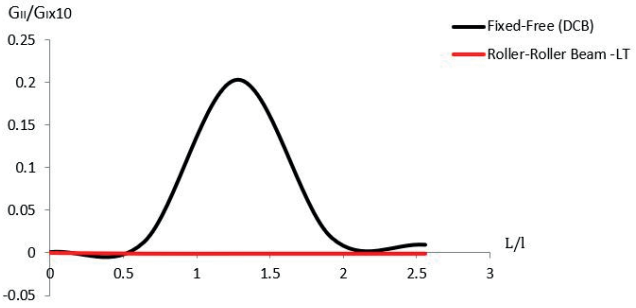

Fig. 11 Ratio of energy release rates G_{II}/G_I for both modes vs. L/l the crack length L normalized by the specimen width l for fixed-free conditions

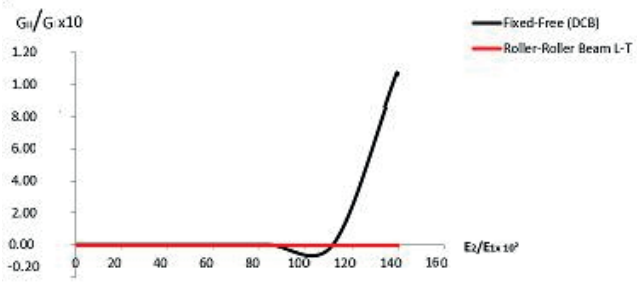

Fig. 12 Ratio of Energy release rates G_{II}/G_I for both modes vs. the relative moduli E_{II}/E_I for various cracks

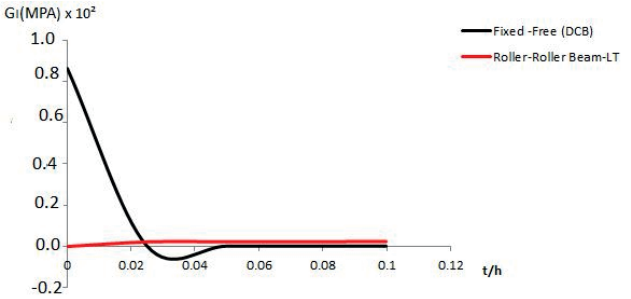

Fig. 13 Energy release rates G_I vs. t/h bond thickness for fixed-free conditions

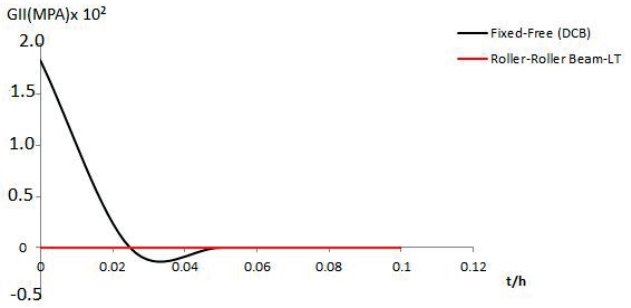

Fig. 14 Energy release rates G_{II} vs. t/h with fixed-free conditions

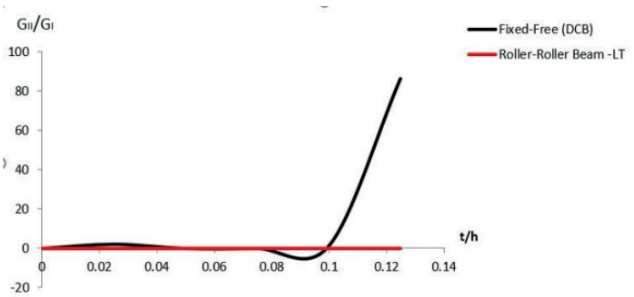

Fig. 15 Energy release rates G_{II}/G_I vs. t/h with fixed-free conditions

In Fig. 15, we notice that contribution of energy G_{II}/G_I to the adhesive layer of the DCB increases for higher ratio of t/h of adhesive at fixed free boundary condition, however; energy's contribution to the adhesive layer at the roller-roller BC is higher for crack's lengths. This contribution gets lower than the energy for fixed free BC.

9 Conclusions

A study of the mechanical behavior of single lap-shear adhesive joints with different overlap lengths was performed. Joints made of laminated composites and aluminum adhesive were tested. Obtained results were compared with those obtained using numerical simulations analysis. These latest including mixed modes I and II were simulated through interface finite elements. Then, the main objective in this study is to verify the adequacy of cohesive damage models for the strength prediction of bonded joints. These models are attractive in modelling fracture problems since they do not require the definition of an initial crack. Besides, these models account for the thickness of the adhesive bond and its elastic properties. In general, a mixed mode cohesive damage model is used to simulate onset and growth in the adhesive layer. It is proven that adhesive joints present several characteristics and offer many advantages when compared to other widely used joining methods.

In this research work, energy release rates set for both modes I and II have been validated for selected results. It is found that the total ERR increases with an increase of the adhesive's thickness, meanwhile; a decrease occurs at the same ratio with the crack's adhesive layer. Then, it is proven that the effects of the adhesive modulus and thickness improve the accuracy of fracture energy assessment particularly for short crack lengths. Notice that thicker is the adhesive layer (order of $t/h \approx 5\%$), more the strength is higher.

Acknowledgements

Authors thank the Built Environment Research Laboratory through the General Direction of Scientific and Development of Technology/MESRS for supporting the work presented here.

References

[1] Goland, M., Reissner, E. "The Stresses in Cemented Joints", Journal of Applied Mechanics, 11(1), pp. A17–A27, 1944. https://doi.org/10.1115/1.4009336

[2] Luo, Q., Tong, L. "Analytical solutions for adhesive composite joints considering large deflection and transverse shear deformation in adherents", International Journal of Solids and Structures, 45, pp. 5914–5935, 2008. https://doi.org/10.1016/j.ijsolstr.2008.07.001

[3] Tsai, M. Y., Morton, J. "An evaluation of analytical and numerical solutions to the single-lap joint", International Journal of Solids and Structures, 31(18), pp. 2537–2563, 1994. https://doi.org/10.1016/0020-7683(94)90036-1

[4] Oplinger, D. W. "Effects of adherend deflections in single lap joints", International Journal of Solids and Structures, 31(18), pp. 2565–2587, 1994. https://doi.org/10.1016/0020-7683(94)90037-X

[5] Hart-Smith, L. J. "Adhesive-bonded Single-Lap Joints", NASA Langley Research Center, Hampton, VI, USA, Rep. CR-112235, 1973.

[6] Ayas, H., Touati, M., Chabaat, M. "Approximate analytical solution for free axial vibration of a cracked cantilever beam", International Journal of Sustainable Building Technology and Urban Development, 11(4), pp. 209–221, 2020. https://doi.org/10.22712/susb.20200016

[7] Kim, S. B., Gurvich, M. R., Robeson, M. R., Lorthridge, D. R. "Progressive damage modeling of thick laminated composites: Robust deterministic and probabilistic implementation", presented at Science in the Age of Experience, 2018 SIMULIA Global User Meeting, Boston, MA, USA, June 18–21, 2018.

[8] Ayas, H., Amara, L., Chabaat, M. "Approximate analytical analysis of longitudinal natural frequencies of a cracked beam", International Journal of Structural Integrity, 12(4), pp. 534–547, 2020. https://doi.org/10.1108/IJSI-07-2020-0065

[9] Grant, L. D. R., Adams, R. D., da Silva, L. F. M. "Experimental and numerical analysis of single-lap joints for the automotive industry", International Journal of Adhesion and Adhesives, 29(4), pp. 405–413, 2009. https://doi.org/10.1016/j.ijadhadh.2008.09.001

[10] Ayas, H., Hamli Benzahar, H., Chabaat, M. "Energy release rate during the cracking of composite materials", Energy Procedia, 74, pp. 1040–1047, 2015. https://doi.org/10.1016/j.egypro.2015.07.742

[11] Ayas, H., Hamli Benzahar, H., Chabaat, M. "Finite element analysis of stress intensity factors in the cracking of brittle materials under biaxial loading", Applied Mechanics and Materials, 834, pp. 67–72, 2016. https://doi.org/10.4028/www.scientific.net/AMM.834.67

[12] Hamli Benzahar, H., Chabaat, M. "Damage Zone Size Limit during the Crack Propagation", Periodica Polytechnica Civil Engineering, 64(1), pp. 73–80, 2020. https://doi.org/10.3311/PPci.14745

[13] Hammoudi, I., Chabaat, M. "Damage propagation at the interface of a sandwich beam", presented at International Conference on 4th Mechanics of Composites, Carlos III University, Madrid, Spain, July, 9–12, 2018.

[14] Lyamine, B. "Analyse Elasto-Plastique des Plaques Minces et Epaisses par Elements Finis" (Elasto-Plastic Analysis of Thin and Thick Plates by Finite Elements), PhD Theis, Université de Annaba, 2004. (in Spanish)

[15] de Moura, M. F. S. F., Campilho, R. D. S. G., Gonçalves, J. P. M. "Mixed-Mode Cohesive Damage Model Applied to the Simulation of the Mechanical Behaviour of Laminated Adhesive Joints", Journal of Adhesion Science and Technology, 23, pp. 1477–1491, 2009. https://doi.org/10.1163/156856109X433036

[16] Schwalbe, K.-H., Scheider, I., Cornec, A. "Guidelines for applying cohesive models to the damage behavior of engineering materials and structures", Springer, Berlin, Heidelberg, Germany, 2012. https://doi.org/10.1007/978-3-642-29494-5

[17] Ibrahim, S. K., Rad, M. M. "Numerical Plastic Analysis of Non-Prismatic Reinforced Concrete Beams Strengthened by Carbon Fiber Reinforced Polymers", In: 13th fib International PhD Symposium in Civil Engineering, Paris, France, 2020, pp. 208–215.

[18] Timoshenko, S., Goodier, J. N. "Theory of Elasticity", 3rd Ed., The Maple Press, York, PA, USA, 1986.

Appendix A

Boundary Conditions

Fixed-Free

$$w_0 = 0,\ \frac{dw_0}{dx} = 0, M_A = P\left(t+\frac{h}{2}\right) - F.B,\ \ R_A = -F, \quad -L < x < 0 \tag{57}$$

$$w_0(L) = w_1(L), w_2 = 0,\ \ \frac{dw_2}{dx} = 0,\ \ 0 < x < l \tag{58}$$

Eq. (10) becomes;

$$w_0 = A_1 \sinh \beta_0 x_0 + A_2 cosh \beta_0 x_0 + \frac{\left(P\left(t+\frac{h}{2}\right) - F.B\right)}{F} - x_0 \tag{59}$$

where;

$$A_1 = \frac{2M_A}{F}\left(\frac{\beta_1^2}{\beta_0^1 - \beta_1^2}\right)\left(\frac{\cosh\beta_0 L - \beta_0 \sinh\beta_0 L}{\beta_0 \cosh\beta_0 L + \sinh\beta_0 L}\right) + \frac{1}{\beta_0 \cosh\beta_0 L + \sinh\beta_0 L}\left(\frac{M_A}{F} + \frac{R_A}{F}(1-L)\right), \tag{60}$$

$$A_2 = \frac{2M_A}{F}\left(\frac{\beta_1^2}{\beta_0^1 - \beta_1^2}\right). \tag{61}$$

Eq. (11) becomes;

$$w_1 = B_1 \sinh \beta_1 x_1 + B_2 \cosh \beta_1 x_1 - \frac{\left(P\left(t+\frac{h}{2}\right) - F.B\right)}{F}, \tag{62}$$

$$B_1 = \frac{2M_A}{F}\left(\frac{\beta_0\beta_1}{\beta_0^1 - \beta_1^2}\right)\left(\frac{\cosh\beta_0 L - \beta_0 \sinh\beta_0 L}{\beta_0 \cosh\beta_0 L + \sinh\beta_0 L}\right) + \left(\frac{\beta_0}{\beta_0\beta_1 \cosh\beta_0 L + \beta_1 \sinh\beta_0 L}\right)\left(\frac{M_A}{F} + \frac{R_A}{F}(1-L)\right), \tag{63}$$

$$B_2 = \frac{2M_A}{F}\left(\frac{\beta_0^2}{\beta_0^1 - \beta_1^2}\right). \tag{64}$$

Constants β_{s1}, β_{a1}

$$\beta_{s1} = \sqrt{2}\sqrt{\beta_\sigma^2 + \sqrt{\beta_\sigma^2 - \beta_k^2}} \tag{65}$$

$$\beta_{s2} = \sqrt{2}\sqrt{\beta_\sigma^2 - \sqrt{\beta_\sigma^2 - \beta_k^2}} \tag{66}$$

$$\beta_{a1}^2 = \frac{1}{2}[(\alpha_a\beta_\tau^2 + \frac{\beta_k^2}{2} + \sqrt{\alpha_a^2\beta_\tau^4 + \left(\alpha_a - \frac{1}{2}\right)\beta_\tau^2\beta_k^2 + \frac{\beta_k^4}{4}} \tag{67}$$

$$\beta_{a2}^2 = \frac{1}{2}[(\alpha_a\beta_\tau^2 + \frac{\beta_k^2}{2} - \sqrt{\alpha_a^2\beta_\tau^4 + \left(\alpha_a - \frac{1}{2}\right)\beta_\tau^2\beta_k^2 + \frac{\beta_k^4}{4}} \tag{68}$$

For isotropic adherend $\alpha_1 = 1$, we get;

$$\beta_{a1}^2 = \frac{1}{2}[(\beta_\tau^2 + \frac{\beta_k^2}{2} + \sqrt{\beta_\tau^4 + \frac{\beta_\tau^2\beta_k^2}{2} + \frac{\beta_k^4}{4}}, \tag{69}$$

$$\beta_{a2}^2 = \frac{1}{2}[(\beta_\tau^2 + \frac{\beta_k^2}{2} - \sqrt{\beta_\tau^4 + \frac{\beta_\tau^2\beta_k^2}{2} + \frac{\beta_k^4}{4}}, \tag{70}$$

where;

$$\beta_\tau = \sqrt{\frac{G_a}{A_1}},\ \ \beta_k = \sqrt{\frac{F}{D_0}},\ \ \beta_\sigma = \frac{\sqrt{2}}{2}\sqrt[4]{\frac{E_a}{t D_0}}, \tag{71}$$

$$B\sigma_1 = \frac{-M_1 a_{22} + V a_{12}}{D(a_{11}a_{22} - a_{12}a_{21})}, \tag{72}$$

$$B\sigma_4 = \frac{-V_1 a_{11} + M a_{21}}{D(a_{11}a_{22} - a_{12}a_{21})}, \tag{73}$$

with;

$$a_{11} = \left(\beta s_1^2 - 4\beta_g^2\right).\cosh\beta_{s1}L, \tag{74}$$

$$a_{12} = \left(\beta s_2^2 - 4\beta_g^2\right).\cosh\beta_{s2}L, \tag{75}$$

$$a_{21} = \beta s_1\left(\beta s_2^2 - 4\beta_g^2\right).\sinh\beta_{s1}L, \tag{76}$$

$$a_{22} = \beta s_2\left(\beta s_2^2 - 4\beta_g^2\right).\sinh\beta_{s2}L. \tag{77}$$